Journal of Applied Polymer Science

Preparation and properties of polyvinyl chloride ultrafiltration membranes blended with functionalized multi-walled carbon nanotubes and MWCNTs/Fe_3O_4 hybrids

Caihong Wang,[1,2] Hao Wu,[3] Fangshu Qu,[1] Heng Liang,[1] Xiaojun Niu,[3] Guibai Li[1]

[1]State Key Laboratory of Urban Water Resource and Environment (SKLUWRE), Harbin Institute of Technology, Harbin 150090, China

[2]The Architecture Design and Research Institute of Guangdong Province, Guangzhou 510100, China

[3]School of Environment and Energy, South China University of Technology, Guangzhou 510006, China

Correspondence to: H. Liang (E-mail: hitliangheng@gmail.com)

ABSTRACT: To investigate the influence of magnetic materials combined with carbon nanotubes (CNTs) as fillers on the membrane properties, multi-walled carbon nanotubes (MWCNTs) functionalized by mixed acids (V_{H2SO4}:V_{HNO3}=3:1) were loaded by Fe_3O_4 through a hydrothermal method. The obtained MWCNTs/Fe_3O_4 hybrids were characterized by X-ray diffraction (XRD), Infrared spectroscopy (IR) spectrum, and scanning electron microscope (SEM) and then blended with polyvinyl chloride (PVC) to prepare ultrafiltration (UF) membranes through a phase inversion process. Simultaneously, two other UF membranes, PVC blended with acid-treated MWCNTs and PVC blended with nothing, were also prepared. The results showed that the membrane porosity and mean pore size increased slightly with the addition of fillers. Static contact angle showed that MWCNTs/Fe_3O_4 hybrids improved the hydrophilicity of membrane surface better than the acid-treated MWCNTs. Pure water flux increased consistently with the hydrophilicity of the membrane surface. SEM and atomic force microscope (AFM) images showed that the MWCNTs/Fe_3O_4 blended membrane formed a relatively complete pore structure throughout the cross-section and had a rougher top surface. However, the mechanical properties of membranes with fillers were reduced compared with the pristine PVC membrane. The rejections of membranes for Bovine serum albumin (BSA), Bisphenol A (BPA), and Norfloxacin (NOR) showed that MWCNTs/Fe_3O_4 played an important role in trapping pollutants in membrane filtration. © 2016 Wiley Periodicals, Inc. J. Appl. Polym. Sci. **2016**, *133*, 43417.

KEYWORDS: blends; membranes; nanoparticles; nanowires and nanocrystals; separation techniques

Received 18 October 2015; accepted 6 January 2016
DOI: 10.1002/app.43417

INTRODUCTION

Membranes have been proven an effective way for separation due to its stability, efficiency, and low-cost requirement.[1] Among various reported membranes, polymeric membrane exhibits a good thermal and mechanical stability and has attracted considerable attention both academically and industrially.

Polyvinyl chloride (PVC) has been considered as an outstanding membrane materials because of its excellent physical and chemical properties.[2] However, polymer membranes such as PVC made through a phase inversion process generally show a reduction of permeate flux at high pressure resulted from the compaction of the original porous structure.[3] In addition, the PVC membrane tends to spontaneous wrinkling and its hydrophobic nature causes severe membrane fouling and permeability decline in filtration. In order to improve membrane performance and structural stability, some inorganic materials such as alumina (Al_2O_3),[4–6] zirconia (ZrO_2),[7,8] silica (SiO_2),[9,10] titaniumdioxide (TiO_2),[11–13] ironoxide (Fe_3O_4).[14–16] carbon nanotubes (CNTs)[1,17–19] have been blended in during the membrane fabrication. For instance, Huang *et al.*[15] reported the fabrication of polyvinylidene fluoride (PVDF)-Fe_3O_4 ultrafiltration (UF) membrane with a magnetic field assisted method and found a novel membrane with lamellar macrovoids in the sublayer, furthermore an improved performance has been observed in pure water flux and initial rejection.

CNTs are tube-like materials made of rolling up graphene sheets. Multi-walled carbon nanotubes (MWCNTs) are composed of multiple layers of graphene sheets, while single-walled carbon nanotubes (SWCNTs) have cylindrical shape consisting of a single graphene shell.[20] Because of its large surface area, high aspect ratio, and low impacts on the environment, CNTs have become one of the most promising materials in water treatment, especially as the fillers in the microfiltration or ultrafiltration

Table I. Detail composition of the Three Membranes

Membrane no.	PVC content (wt %)	Acid-treated MWCNTs content (wt %)	MWCNTs/Fe_3O_4 content (wt %)	DMAC content (wt %)	PVP content (wt %)
PVC-I	14	0	0	85	1
PVC-II	14	0.3	0	84.7	1
PVC-III	14	0	0.65[a]	84.35	1

[a]Including 0.3 wt % acid-treated MWCNTs.

membranes. Majeed *et al.*[18] blended hydroxyl functionalized MWCNTs with polyacrylonitrile (PAN) to prepare ultrafiltration membrane and found the addition of MWCNTs not only improved polymer solution viscosity, the water flux, tensile strength, but also reduced the compaction of the membrane significantly under high pressures. Qiu *et al.*[19] prepared ultrafiltration membrane by blending MWCNTs functionalized by isocyanate and isophthaloyl chloride with polysulfone (PSF). The results showed that the MWCNTs influenced surface mean pore size and porosity of membrane and facilitated the reduction of the fouling from protein adsorption. The incorporation with either CNTs or magnetic particles could greatly improve the performance of the membranes, but these membranes still have their own drawbacks in electrochemical, magnetic, or biocompatible properties, which hinder their further applications. Interests might be to fabricate the membrane blended with both of them. Due to strong interaction between CNTs and magnetic particles, the membrane with desirable properties perhaps can be obtained. Up to now, various methods have been reported for the fabrication of the CNTs/Fe_3O_4 nanocomposites. For example, Jia *et al.*[21] have successfully obtained necklace-like nanostructures with Fe_3O_4 beads, which were self-assembled along multi-walled carbon nanotubes (MWCNTs) through a simple hydrothermal method. Li *et al.*[22] found the CNTs/Fe_3O_4 nanocomposites exhibited strong adsorption behavior for Bisphenol A (BPA) in aqueous solution. These all prove that CNTs/Fe_3O_4 hybrids have excellent properties in electrochemistry, magnetism, or adsorption properties for some special molecules.

Unfortunately, few reports have applied the excellent properties of CNTs/Fe_3O_4 in preparation membrane. In this work, functionalized MWCNTs loading Fe_3O_4 were fabricated and then the products were blended with PVC to prepare ultrafiltration membrane. The membrane morphology, contact angle, porosity, and mean pore size were examined and the rejections for Bovine serum albumin (BSA), BPA, and Norfloxacin (NOR) were investigated.

METHODOLOGY AND MATERIALS

Materials

Multi-walled carbon nanotubes (MWCNTs, with diameters of 10–20 nm, 97% purity, and specific surface area 100–160 m^2/g) were provided by Shenzhen Nanotech Port Co., China. Polyvinylpyrrolidone (PVP) with molecular weight of 10,000 was purchased from Tianjin Damao Chemical Reagent Company. Polyvinylchloride (PVC) was supplied by Xiya Reagent Company. Bovine serum albumin (BSA), Bisphenol A (BPA), and Norfloxacin (NOR) were purchased from Aladdin Industrial Corporation (China). *N*,*N*-dimethylacetamide (DMAC), Ferrous sulfate ($FeSO_4{\cdot}7H_2O$), and Ferric chloride ($FeCl_3{\cdot}6H_2O$) were analytical grade.

Preparation and Characterization of MWCNTs/Fe_3O_4

In order to increase its purity and activity, the MWCNTs were ultrasonically treated with a mixture of concentrated acid (V_{H2SO4}:V_{HNO3} = 3:1) for 4 h at 65 °C. Then the solution was diluted with deionized water, filtered to neutral through a 0.45 μm membrane, and then dried in vacuum for 12 h. MWCNTs/Fe_3O_4 hybrids were prepared through a hydrothermal method as described by Hou *et al.*[23] Briefly, $FeCl_3$ and $FeSO_4$ (molar ratio 2:1) and 0.5 g acid-treated MWCNTs were ultrasonically mixed with 400 mL deionized water. Under N_2 flow, the solution was stirring at 50 °C for 0.5 h, and then continued stirring at 65 °C for 1 h under pH=12. The obtained precipitates were filtered, rinsed with deionized water to neutral, dried, and milled.

X-ray diffraction (XRD, Empyrean, PANalytical; with Cu Kα radiation) was used to identify the phase structure. Infrared spectroscopy (IR, Thermo Nicodet 6700, Thermo Electron Corporation) was used to identify the functional groups of acid-treated MWCNTs and MWCNTs/Fe_3O_4 by mixing the nanocomposites with KBr and pressing into pellets. Scanning electron microscope (SEM, Merlin, Carl Zeiss) was employed for examination of the morphology of the products.

Preparation of Membrane

UF membranes named PVC-I, PVC-II, PVC-III were prepared via a phase inversion method.[19] The composition of the membranes was shown in Table I.

For the preparation of PVC-II and PVC-III, acid-treated MWCNTs or MWCNTs/Fe_3O_4 hybrids were ultrasonically mixed with DMAC, followed by addition of PVC and PVP under stirring. The casting solution was stirred at room temperature for 12 h and was kept in the dark for 12 h to remove air bubbles. Then the casting solution was spread into membranes on a glass plate with a membrane applicator, and then the membranes evaporated in air for 1 min before immersing into deionized water coagulation bath. The membranes were kept in water at room temperature for 24 h before further use. The preparation of PVC-I was performed with the procedure similar to that of PVC-II and PVC-III by adding PVC and PVP directly into DMAC to get the casting solution.

Characterization of Membrane

Morphology Observation. The surfaces and cross-sectional structures of membranes were examined by scanning electron microscope (SEM, Merlin, Carl Zeiss). Cross-section structures were prepared by being fractured in the liquid nitrogen. Samples were coated with a thin layer of Au/Pd before analysis. Atomic force microscope (AFM, Cypher S, Asylum Research) was used to observe surface morphology and roughness of the membranes without special sample preparation. Simply about 1 cm^2 pieces of membranes were prepared and glued on the glass substrate before being scanned.

Porosity and Mean Pore Size. The membrane porosity, $\varepsilon(\%)$, was determined by gravimetric method[17] using the expression given in eq. (1).

$$\varepsilon(\%)=\frac{(w_1\text{-}w_2)/d_w}{(w_1\text{-}w_2)/d_w+w_2/d_p}\times 100\% \quad (1)$$

where w_1 was the weight of the wet membrane (g), w_2 was the weight of the dry membrane (g), d_w was the pure water density (0.998 g/cm^3), and d_p was the polymer density (as the inorganic content in the membrane matrix was small and d_p was approximate to d_{PVC}, namely 1.4 g/cm^3).[2]

The mean pore size (nm) was calculated via filtration velocity method. It was expressed by the Guerout-Elford-Ferry equation [detail in eq. (2)], which represented the average pore size along the membrane thickness.[24,25]

$$r_m=\sqrt{\frac{(2.9-1.75\varepsilon)8\eta\theta Q}{\varepsilon A\Delta P}} \quad (2)$$

where η was the pure water viscosity (8.9×10^{-4} Pa s), θ was the membrane thickness (m), Q was the volume of the permeation of pure water per unit time (m^3/s), A was the effective area of membrane (m^2), and ΔP is the operation pressure (100 kPa).

Contact Angle, Pure Water Flux, and Rejection Measurements. A contact angle goniometer (OCA15, Dataphysics) was used to characterize hydrophilicity of the membrane surface. About 1 μL deionized water was dropped onto a dry membrane surface and five measurements at different sites were averaged to get the final data.

The pure water flux and rejection measurements were conducted with a dead-end UF test system at room temperature with the pressure of 0.1 MPa. All membranes were pre-pressured at 0.1 MPa using the pure water for 15 min, and then the pure water fluxes and rejections of BSA, BPA, and NOR were measured.

The concentrations of BSA, BPA, and NOR in the permeation and feed solution were determined by an UV/vis spectrophotometer (8453, Agilent). The pure water flux and rejection were calculated given in eqs. (3) and (4), respectively.

$$F=\frac{V}{A\times T} \quad (3)$$

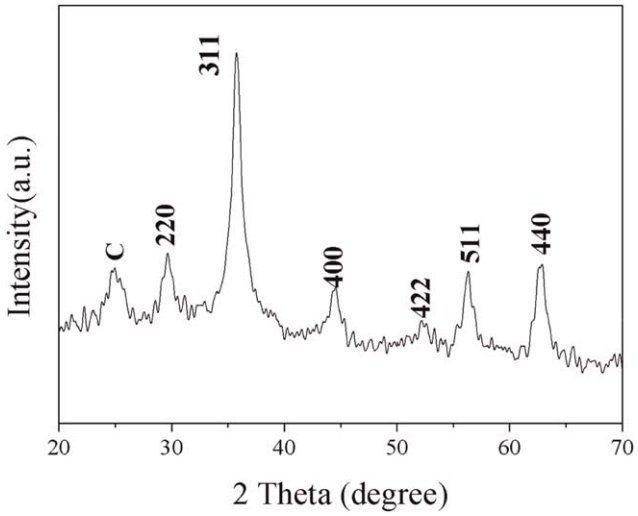

Figure 1. XRD pattern of MWCNTs/Fe_3O_4 hybrids.

$$R=\left(1-\frac{C_P}{C_F}\right)\times 100 \quad (4)$$

where F was the water flux of membrane for pure water (L/m^2 h), V was the volume of permeating pure water (L), $T$was the permeation time (h), R was the rejection ratio (%), and C_P and C_F were the concentrations in the permeation and feed solution, respectively.

Mechanical Properties. The mechanical properties involving tensile strength, elongation at break, and Young's modulus were measured through a universal mechanical testing machine (5697, INSTRON). The samples of 10 cm effective length and 1.5 cm width were conducted with the tensile rate at 5 mm/min. Each membrane was performed five times and the averaged was taken as the final result.

RESULTS AND DISCUSSION

Characterization of MWCNTs/Fe_3O_4

Figure 1 displays XRD patterns of the MWCNTs/Fe_3O_4 hybrids. The peak at 26.1° could be indexed to the diffraction of MWCNTs, indicating the structural integrity of MWCNTs. According to JCPDS NO.89-0691, the diffraction peaks at 30.1°, 35.5°, 43.2°, 53.7°, 57.3°, and 62.8° could be attributed to (220), (311), (400), (422), (511), and (440) crystal planes of cubic Fe_3O_4, respectively. No other peaks were observed indicating the purity of the Fe_3O_4 products.

Figure 2 shows the IR spectra of pristine MWCNTs, acid-treated MWCNTs, and MWCNTs/Fe_3O_4. The emergence of new peaks at 3438 cm^{-1} in acid-treated MWCNTs and 3429 cm^{-1} in MWCNTs/Fe_3O_4 which corresponded to the O–H vibration indicated that the acid pre-treatment had led to the functionalization of MWCNTs with the –OH groups. The peaks in the vicinity of 1600 cm^{-1} could be attributed to the combined vibration of –COOH and C=C bonds. The significantly enhanced absorption peaks in this position for acid-treated MWCNTs and MWCNTs/Fe_3O_4 suggested that carboxyl groups were successfully introduced onto MWCNTs. The appearance of a hump at 574 cm^{-1} in MWCNTs/Fe_3O_4 was considered as the

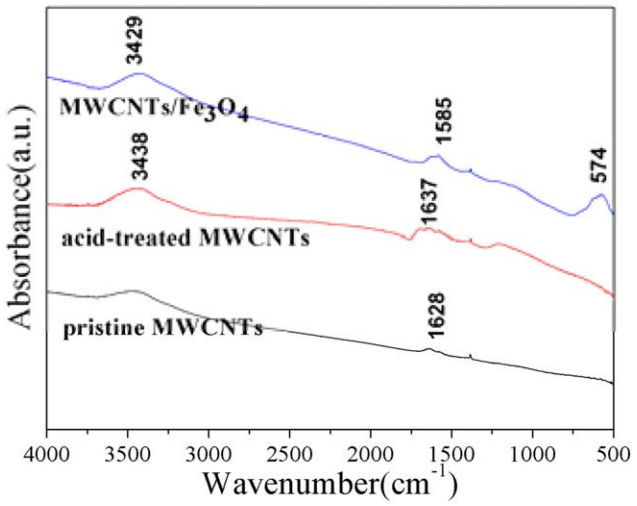

Figure 2. IR spectrum of pristine MWCNTs, acid-treated MWCNTs, and MWCNTs/Fe_3O_4. [Color figure can be viewed in the online issue, which is available at wileyonlinelibrary.com.]

stretching vibration of Fe–O, indicating the presence of the Fe_3O_4 nanoparticles on the surface of MWCNTs, which was well consistent with the XRD results shown above.

The morphologies of acid-treated MWCNTs and MWCNTs/Fe_3O_4 were investigated by SEM. As shown in Figure 3(a), the acid-treated MWCNTs are intertwined with no observable impurity. Figure 3(b) presents a great number of Fe_3O_4 nanoparticles on the surface of MWCNTs, due to the magnetic attraction these Fe_3O_4 nanoparticles are clustered together.

Membrane Morphologies

The top surface and cross-section morphologies of the prepared membranes are given in Figure 4, which showed that the additions of acid-treated MWCNTs and MWCNTs/Fe_3O_4 improved the formation of macro-voids in surfaces. In addition, the membrane containing acid-treated MWCNTs (PVC-II) had the maximum number of macro-voids in surface (see in Figure 4(c)). This could be attributed to the obstruction of the hydrophilic fillers, which made the interaction between solvent and non-solvent declined and the exchange rate between them accelerated during phase inversion process.[17]

In terms of the cross-section morphologies, three membranes manifested the similar asymmetry, and they were changed obviously by the addition of fillers in pore size and pore density. The pores of PVC-III [Figure 4(f)] in sub-layer were formed larger and more completely than PVC-I and PVC-II. The enlarged pores might be the outcome of the fusion of small pores as the increasing viscosity of casting solution.[18] The reason for the relatively complete pore structure might be the addition of MWCNTs/Fe_3O_4 hybrids, which played a supporting role in the formation of pores. We also could see that the pores of top surfaces were the densest for all PVC membranes. It might be attributed to the evaporation in air, which induced the membranes to form a dense layer near the top surface, exerting the major contribution to filtration.

A problem for casting membrane with nanoparticles was the dispersion of the addition. Figure 3 illustrated that in some sites there was a cluster in acid-treated MWCNTs and MWCNTs/Fe_3O_4 hybrids. In the casting solution, the addition of fillers would work as the nucleus and induce the generation of nodular structures in PVC membranes, as shown in Figure 4(g). The spherulites restrained the performance of the fillers. The more the nucleuses, the more the spherulites generated.[26] This phenomenon was adverse to the rejection of membranes.

Figure 5 depicts the three-dimensional AFM images of the top surfaces of the prepared membranes, and the corresponding parameters including mean roughness (R_a), root mean square (R_q), and mean difference between highest peaks and lowest valleys (R_z) are shown in Table II. We can see that the surface roughness was greatly boosted by the addition. This might be due to the larger size and the greater quantity of pores in membranes' surfaces as shown above. The increase in pore size and quantity all had a positive influence on surface roughness.[27] An alternative reason might be due to the existence of the nanoparticles on the membrane surfaces, which promoted the formation of humps and valleys. Rougher surface would be in favor of permeation and hydrophilicity.[17]

Porosity and Mean Pore Size

The porosity and mean pore size are calculated via eqs. (1) and (2), respectively. From Table II, the porosity and mean pore size increased slightly with the addition of fillers. This could be explained as follows: first, the accelerated exchange rate between

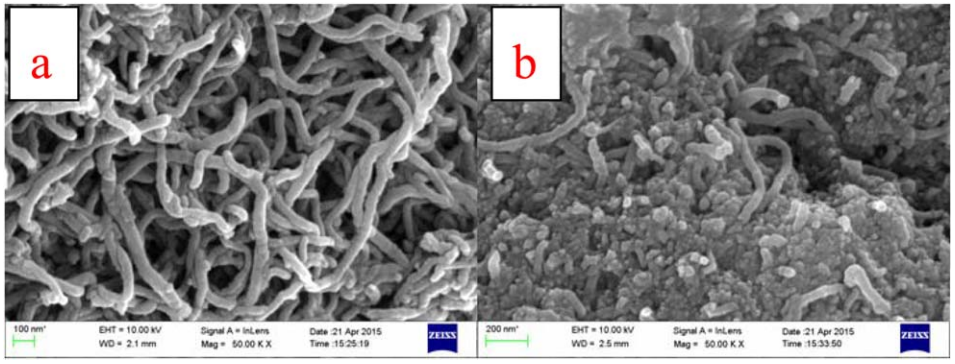

Figure 3. SEM images of (a) acid-treated MWCNTs and (b) MWCNTs/Fe_3O_4. [Color figure can be viewed in the online issue, which is available at wileyonlinelibrary.com.]

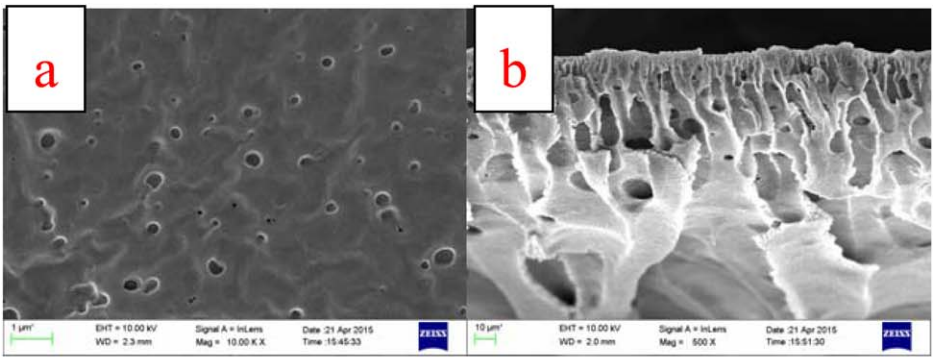

PVC- I

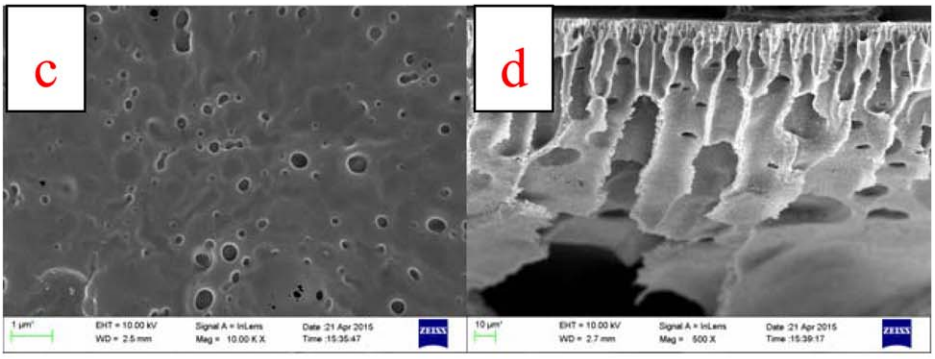

PVC- II

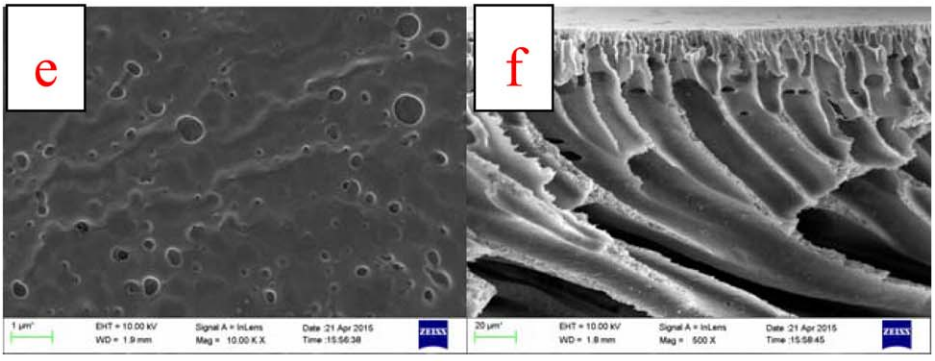

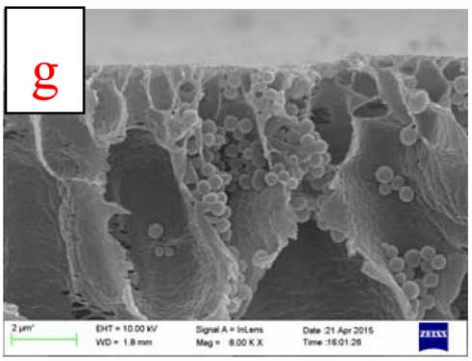

PVC-III

Figure 4. SEM images of top surface (a,c) and (e) and cross-section (b,d,f) and (g) of PVC-I, PVC-II, and PVC-III. [Color figure can be viewed in the online issue, which is available at wileyonlinelibrary.com.]

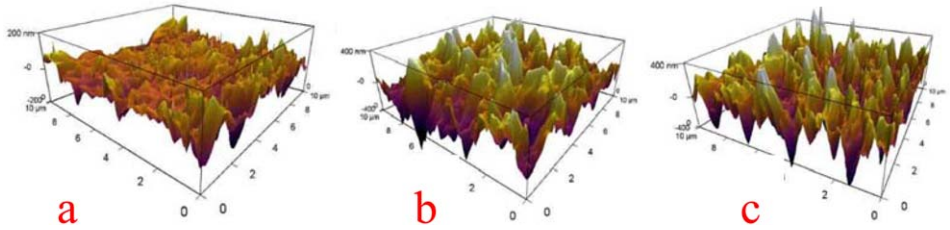

Figure 5. AFM images of top surface of (a) PVC-I, (b) PVC-II, and (c) PVC-III. [Color figure can be viewed in the online issue, which is available at wileyonlinelibrary.com.]

solvent and non-solvent during phase inversion would influence the formation of porosity and mean pore size as discussed previously. Second, the addition of fillers increased the heterogeneity of the membranes. Hydrophilic nanoparticles mixed with polymer matrix could increase the amorphous nature of membranes, enhance the volume fraction among the polymer chains, and then increase the amount of voids and cavities throughout the membrane matrix.[25]

Contact Angle, Pure Water Flux, and Rejection Measurements

The hydrophilicity of membrane surfaces were compared through contact angle measurement. The static contact angles of the three membranes are illustrated in Figure 6. It was observed that the membranes with fillers had a lower contact angle, suggesting that PVC-II and PVC-III had stronger hydrophilicity. This could be due to the incorporation of the acid-treated MWCNTs, which had hydrophilic functional groups. Compared PVC-II with PVC-III, the contact angles decreased from 69.6° to 63.5°. Two reasons contributed to the decrease. One was that Fe_3O_4 as nanoparticle had a relatively better hydrophilicity,[28] thus the hydrophilicity of PVC-III was the combined effects of acid-treated MWCNTs and Fe_3O_4. Another reason was that MWCNTs/Fe_3O_4 was more inclined to exist on the membrane surface during phase inversion process because of its bigger size than acid-treated MWCNTs.

The pure water flux is related strongly with mean pore size, porosity, hydrophilicity, and skin layer. As previously discussed, these parameters changed in the direction of increasing the pure water flux with the addition of fillers, increase in mean pore size, porosity, and decrease in contact angle. Certainly, the pure water fluxes of PVC-I, PVC-II, and PVC-III increased sequentially and reached to 90.4 ± 6.2, 111.7 ± 4.9, and 118.3 ± 7.0 L/m^2 h (shown in Figure 6), respectively.

The rejections of membranes were examined using BSA, BPA, and NOR under the pressure of 0.1 MPa. The concentrations in the permeation and feed solution were measured and the rejections were calculated by eq. (4). Figure 7 depicts the results of the prepared membranes in filtering the three targets. The membranes with additions (PVC-II and PVC-III) had higher rejections than the pristine membrane (PVC-I). Generally, the hydrophilicity of the addition improved the rejection performance of membranes. The rejections of BSA and BPA by PVC-III were $74.6 \pm 1.6\%$ and $57.4 \pm 1.9\%$, which were higher than those by PVC-II (the rejections of BSA and BPA were $73.2 \pm 2.6\%$ and $50.2 \pm 2.2\%$). The slight increases in rejections of BSA and BPA could be attributed to various reasons. Firstly, the increase in hydrophilicity of PVC-III improved the anti-fouling property and the rejection positively by allowing the permeation of more water molecules through the membrane without enhancing the permeability of pollutants.[18] Secondly, the rejections decreased with the increase of mean pore size and porosity. Thirdly, the aggregated clusters of MWCNTs/Fe_3O_4 hybrids gave some flaws in the membrane, which created some special transfer paths for water and pollutants.

The rejection of NOR decreased from $22.9 \pm 1.7\%$ of PVC-II to $18.2 \pm 2.0\%$ of PVC-III. The reason might be that the acid-treated MWCNTs had special adsorption effects on NOR,[29,30] while Fe_3O_4 inhibited the performance of MWCNTs in PVC-III.

Table II. Description on the Roughness Parameters, Porosity, and Mean Pore Size of the Three Membranes

	Roughness				
Membrane no.	R_a (nm)	R_q (nm)	R_z (nm)	Porosity (%)	mean pore size (nm)
PVC-I	43.77	57.58	565.07	82.8 ± 1.1	33.1 ± 1.1
PVC-II	145.73	183.15	1421.24	85.6 ± 1.7	35.6 ± 0.8
PVC-III	147.24	190.36	1411.32	86.4 ± 0.6	36.3 ± 1.1

Mechanical Properties

Table III shows the influence of fillers on mechanical properties of membranes. Tensile strength at break, elongation at break, and Young's modulus were tested. The results showed that the addition of fillers reduced the maximum tensile strength and

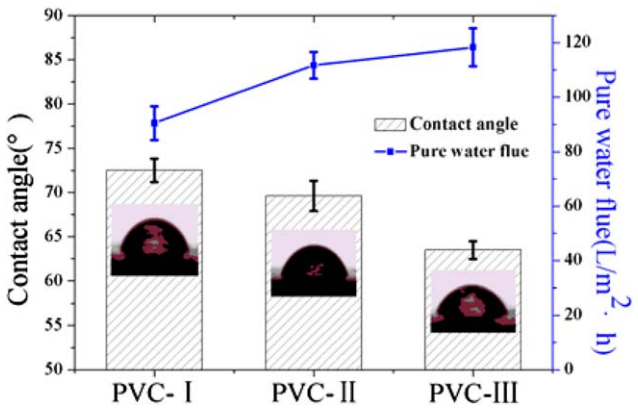

Figure 6. Contact angle, pure water flue of PVC-I, PVC-II, and PVC-III. [Color figure can be viewed in the online issue, which is available at wileyonlinelibrary.com.]

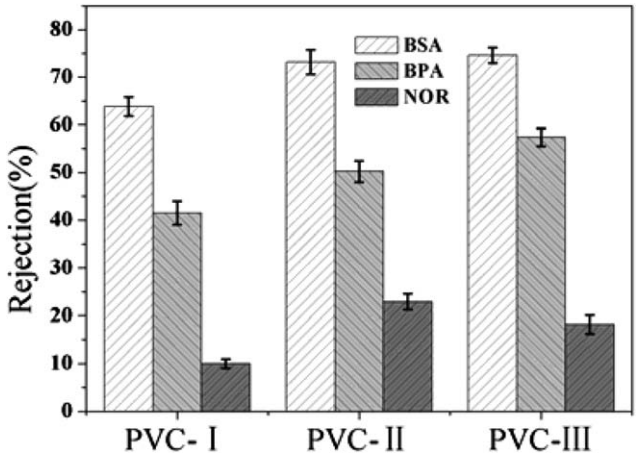

Figure 7. Rejection of PVC-I, PVC-II, and PVC-III for BSA, BPA, and NOR.

elongation at break, since it produces more porosity and larger mean pore size.[2] This was in good agreement with the results shown by Majeed *et al.*[18] and Scharnagl and Buschatz.[31] In addition, Table III showed that PVC-III had a slightly better mechanical property than PVC-II in tensile strength and elongation, suggesting that MWCNTs/Fe_3O_4 hybrids were better membrane material additives than acid-treated MWCNTs. Comparison of the Young's modulus of the three ultrafiltration membranes showed that the addition of fillers increased the rigidity of membranes.

CONCLUSIONS

In summary, acid-treated MWCNTs, which were terminated with oxygenous groups such as carboxyl and hydroxyl, had been used in the depositing process of Fe_3O_4. The obtained MWCNTs/Fe_3O_4 were then used as the fillers to modify the PVC membranes. The results showed that the membranes with MWCNTs/Fe_3O_4 (PVC-III) displayed superior properties to the pristine membranes (PVC-I) and those with acid-treated MWCNTs (PVC-II). Specifically, the PVC-III had the higher porosity, larger mean pore size, rougher top surface and stronger hydrophilicity. Although the addition of MWCNTs/Fe_3O_4 reduced the tensile strength and elongation of membranes, it formed in membrane with a relatively complete pore structure throughout the cross-section. Due to its specific porous structure, the pure water flux of the PVC-III increased from 90.4 ± 6.2 L/m^2 h (for PVC-I) to 118.3 ± 7.0 L/m^2 h and the rejections of PVC-III for BSA, BPA, and NOR increased by 16.9%, 38.3%, and 81.8%, respectively, compared with PVC-I. Comparing PVC-III with PVC-II, PVC-III had a superior rejection than PVC-II for BPA while PVC-II had relatively higher rejection for NOR. It could be seen different fillers could be specifically for different pollutants.

Table III. Mechanical Properties of the Three Membranes

Membrane no.	Tensile strength (MPa)	Elongation at break (%)	Young's modulus (MPa)
PVC-I	2.27 ± 0.17	22.78 ± 5.00	41.10 ± 12.62
PVC-II	1.94 ± 0.13	13.17 ± 2.77	60.59 ± 11.65
PVC-III	2.06 ± 0.13	15.93 ± 1.09	56.70 ± 5.40

ACKNOWLEDGMENTS

This work was supported by the National Natural Science Foundation of China (No. 41071305), Student Research Project of South China University (2015), State Key Laboratory of Pollution Control and Resource Reuse (No. PCRRF14006), and State Key Lab of Subtropical Building Science, South China University of Technology (2014KB13).

REFERENCES

1. Ismail, A. F.; Goh, P. S.; Sanip, S. M.; Aziz, M. *Sep. Purif. Technol.* **2009**, *70*, 12.
2. Xu, J.; Xu, Z. *J. Membr. Sci.* **2002**, *208*, 203.
3. Ebert, K.; Fritsch, D.; Koll, J.; Tjahjawiguna, C. *J. Membr. Sci.* **2004**, *233*, 71.
4. Maximous, N.; Nakhla, G.; Wan, W.; Wong, K. *J. Membr. Sci.* **2009**, *341*, 67.
5. Yan, L.; Li, Y. S.; Xiang, C. B.; Xianda, S. *J. Membr. Sci.* **2006**, *276*, 162.
6. Yan, L.; Li, Y. S.; Xiang, C. B. *Polymer* **2005**, *46*, 7701.
7. Maximous, N.; Nakhla, G.; Wan, W.; Wong, K. *J. Membr. Sci.* **2010**, *352*, 222.
8. Bottino, A.; Capannelli, G.; Comite, A. *Desalination* **2002**, *146*, 35.
9. Wu, H.; Mansouri, J.; Chen, V. *J. Membr. Sci.* **2013**, *433*, 135.
10. Liu, X.; Peng, Y.; Ji, S. *Desalination* **2008**, *221*, 376.
11. Mozia, S.; Szymański, K.; Michalkiewicz, B.; Tryba, B.; Toyoda, M.; Morawski, A. W. *Sep. Purif. Technol.* **2015**, *142*, 137.
12. Mozia, S.; Darowna, D.; Orecki, A.; Wróbel, R.; Wilpiszewska, K.; Morawski, A. W. *J. Membr. Sci.* **2014**, *470*, 356.
13. Rabiee, H.; Farahani, M. H. D. A.; Vatanpour, V. *J. Membr. Sci.* **2014**, *472*, 185.
14. Cleveland, V.; Bingham, J.; Kan, E. *Sep. Purif. Technol.* **2014**, *133*, 388.
15. Huang, Z.; Zheng, F.; Zhang, Z.; Xu, H.; Zhou, K. *Desalination* **2012**, *292*, 64.
16. Jian, P.; Yahui, H.; Yang, W.; Linlin, L. *J. Membr. Sci.* **2006**, *284*, 9.
17. Ma, J.; Zhao, Y.; Xu, Z.; Min, C.; Zhou, B.; Li, Y.; Li, B.; Niu, J. *Desalination* **2013**, *320*, 1.
18. Majeed, S.; Fierro, D.; Buhr, K.; Wind, J.; Du, B.; Boschetti-de-Fierro, A.; Abetz, V. *J. Membr. Sci. 403–404*, 101.
19. Qiu, S.; Wu, L.; Pan, X.; Zhang, L.; Chen, H.; Gao, C. *J. Membr. Sci.* **2009**, *342*, 165.
20. Das, R.; Abd Hamid, S. B.; Ali, M. E.; Ismail, A. F.; Annuar, M. S. M.; Ramakrishna, S. *Desalination* **2014**, *354*, 160.
21. Jia, B.; Gao, L.; Sun, J. *Carbon* **2007**, *45*, 1476.

22. Li, S.; Gong, Y.; Yang, Y.; He, C.; Hu, L.; Zhu, L.; Sun, L.; Shu, D. *Chem. Eng. J.* **2015**, *260*, 231.
23. Hou, C.; Li, T.; Zhao, T.; Liu, H.; Liu, L.; Zhang, W. *New Carbon Mater.* **2013**, *28*, 184.
24. Zhang, G.; Lu, S.; Zhang, L.; Meng, Q.; Shen, C.; Zhang, J. *J. Membr. Sci.* **2013**, *436*, 163.
25. Yuliwati, E.; Ismail, A. F.; Matsuura, T.; Kassim, M. A.; Abdullah, M. S. *Desalination* **2011**, *283*, 206.
26. Cui, Z.; Hassankiadeh, N. T.; Lee, S. Y.; Lee, J. M.; Woo, K. T.; Sanguineti, A.; Arcella, V.; Lee, Y. M.; Drioli, E. *J. Membr. Sci.* **2013**, *444*, 223.
27. Ng, L. Y.; Mohammad, A. W.; Leo, C. P.; Hilal, N. *Desalination* **2013**, *308*, 15.
28. Ghaemi, N.; Madaeni, S. S.; Daraei, P.; Rajabi, H.; Zinadini, S.; Alizadeh, A.; Heydari, R.; Beygzadeh, M.; Ghouzivand, S. *Chem. Eng. J.* **2015**, *263*, 101.
29. Yang, W.; Lu, Y.; Zheng, F.; Xue, X.; Li, N.; Liu, D. *Chem. Eng. J.* **2012**, *179*, 112.
30. Peng, H.; Pan, B.; Wu, M.; Liu, Y.; Zhang, D.; Xing, B. *J. Hazard. Mater.* **2012**, *233–234*, 89.
31. Scharnagl, N.; Buschatz, H. *Desalination* **2001**, *139*, 191.